Effect of electron/hole doping on the transport properties of lanthanum manganites LaMnO$_3$

Effect of electron/hole doping on the transport properties of lanthanum manganites LaMnO₃

Dinesh Varshney[1,3], I Mansuri[1] and N Kaurav[2]

[1] School of Physics, Devi Ahilya University, Khandwa Road Campus, Indore 452001, India
[2] Department of Physics, Institute of Science and Laboratory Education, IPS Academy, Indore 452012, India

E-mail: vdinesh33@rediffmail.com

Abstract
We report the results of electrical resistivity, magnetic susceptibility and thermoelectric power measurements on the stoichiometric hole-doped $La_{0.8}Ca_{0.2}MnO_3$ and electron-doped $La_{0.8}Ce_{0.2}MnO_3$ manganites. The resistivity and thermopower data show a metal–insulator phase transition for both samples. Magnetic susceptibility measurement confirms that both the samples undergo a transition from paramagnetic to ferromagnetic phase at defined Curie temperatures T_c = 240 K ($La_{0.8}Ca_{0.2}MnO_3$) and 263 K ($La_{0.8}Ce_{0.2}MnO_3$). The electrical resistivity data are then theoretically analysed within the framework of the classical electron–phonon model of resistivity, i.e. the Bloch–Gruneisen model. Detailed analysis of the electrical resistivity of electron- and hole-doped manganites suggests that besides the electron–phonon effect another possibility for the change in carrier density arises due to the presence of electron correlation in the metallic system. From the thermopower $S(T)$ results, we suggest that its behaviour is determined by competition among the several operating scattering mechanisms for the heat carriers and a balance between carrier diffusion and phonon drag contributions in the polycrystalline samples of hole-doped $La_{0.8}Ca_{0.2}MnO_3$ and electron-doped $La_{0.8}Ce_{0.2}MnO_3$ manganites.

1. Introduction

The hole-doped manganites $La_{1-x}Ca_xMnO_3$ corresponding to x smaller than $1/2$ have been the purpose of numerous investigations in recent years owing to their colossal magnetoresistance (CMR) properties [1]. This behaviour has been interpreted on the basis of the double-exchange theory (DE) [2] and of the dynamic Jahn–Teller (JT) effect [3]. Detailed investigations evidenced strong electron–phonon coupling due to JT ions, which plays a key role in the

---

[3] Author to whom any correspondence should be addressed.

transport mechanism of these manganites [4]. Relatively less studied in this respect are the electron-doped manganites of the form $La_{1-x}Ce_xMnO_3$. It is noticed that Ce enters these compounds in the 4^+ valence state and therefore one expects these to have certain unique properties. Thus, a detailed understanding of the transport properties is essential for electron- and hole-doped manganites.

The resistivity as a function of temperature in the doped manganites exhibits three regimes: low-temperature metallic-like conduction with an unexpectedly large absolute value of the resistivity, an abrupt drop in resistivity associated with magnetic ordering, and high-temperature activated conduction. The current consensus is to interpret the temperature dependence of resistivity in the ferromagnetic metallic regime, believed to be intrinsic, as a consequence of electron–electron [5], electron–phonon [4], and electron–magnon scattering [6] processes. Zhao *et al* [7] have reported the resistivity data of $La_{1-x}Ca_xMnO_3$ and predict that small polaron transport is the prevalent conduction mechanism below 100 K. Polaron mechanisms demonstrate the lowest optical modes to be significant for resistivity, in contrast to the recent Raman spectroscopy measurements [8].

The frequency and field dependence of real and imaginary parts of ac susceptibility (ac-χ) has become an established tool for investigating magnetic materials. The ac-χ measurements reveal a complex behaviour of hole doped manganites. $CaMnO_3$ exhibits a weak ferromagnetic component ($T_c = 122$ K) whereas for $Ca_{1-x}Sm_xMnO_3$ ($0 \leqslant x \leqslant 0.12$) the $\chi'(T)$ curves are characterized by large bumps below T_c [9]. Later on, Mandal and Ghosh [10] also measured the ac susceptibility of hole doped manganites to see the effect of structural transition on magnetic properties. Both real (χ') and imaginary (χ'') parts of the ac susceptibility increase sharply at T_c and show a peak just below T_c.

In the low-temperature metallic phase, like resistivity, thermopower is also related to the changes in electronic structure and different scattering processes. Jaime *et al* [4] measured the thermopower $S(T, H)$ and resistivity $\rho(T, H)$ of laser-ablated $La_{0.67}Ca_{0.33}MnO_3$ films, as a function of temperature and external magnetic field. On heating, a metal–insulator transition occurs at temperatures below the resistivity peak, observed via a jump between a low-T regime, where $S \propto T$, and a high-T regime, where $S \propto 1/T$. Fisher and co-workers [11] have analysed the complex phase diagram of $L_{1-x}Ca_xMnO_3$ (L = Pr, Nd) that shows the existence of several charge and magnetically ordered states. They argued that the changes in the electronic structure occur at the transitions between the various phases in the temperature dependence of the absolute thermopower. Later on Hundley *et al* [12] measured the temperature-dependent S of $La_{1-x}Ca_xMnO_{3+\delta}$. The analysis of thermoelectric power is within the framework of an adiabatic small polaron to determine the number of charge carriers per active transport site in the paramagnetic state.

As mentioned above, in divalent-ion-doped manganites, the manganese ion exists in trivalent and tetravalent states, but if the rare-earth ion is partially replaced by some tetravalent ion the corresponding amount of manganese will be converted into a divalent state. It is essential to check that the DE mechanism will be inhibited if a tetravalent ion is doped. Also, the thermoelectric power depends on the way the heat carriers in different bands of different dimensionality interact with one another and with the environment, namely the possible interaction of phonons with defects, grain boundaries and by themselves. It is worth mentioning that in the above-mentioned studies [3–12], the importance of the competition among the several operating scattering mechanisms and a balance between the phonon drag and carrier diffusive contributions have not been stressed. However, these are believed to be substantial to clarify the heat transfer.

In order to understand these issues, we present our results of resistivity, magnetic susceptibility and thermopower measurements on hole-doped $La_{0.8}Ca_{0.2}MnO_3$ and electron-

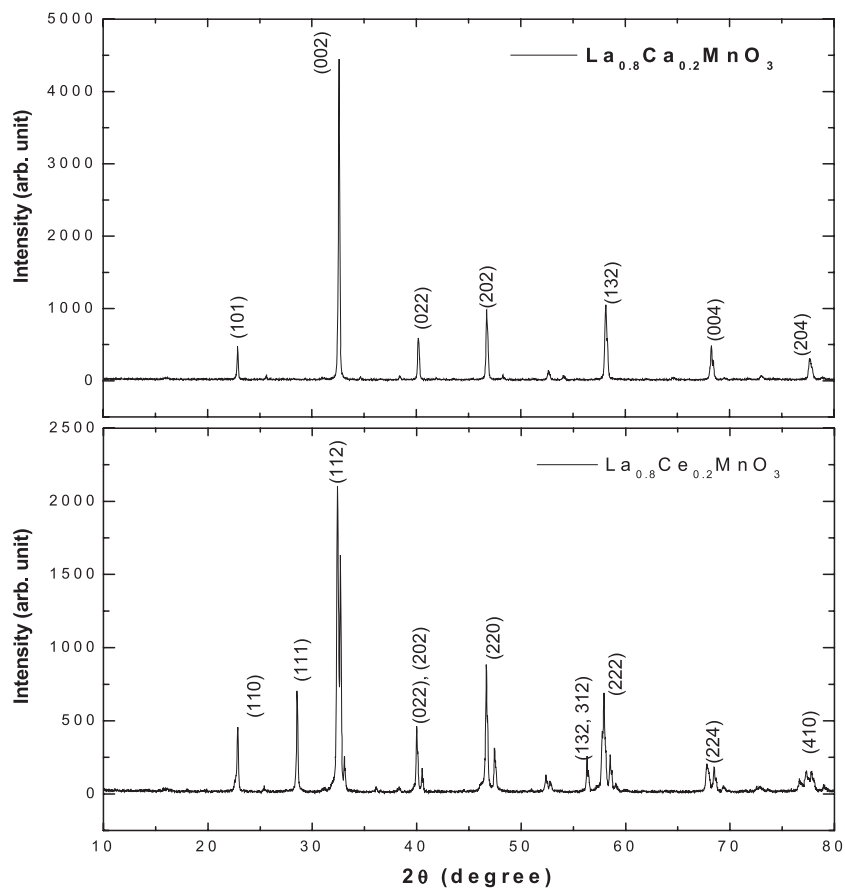**Figure 1.** X-ray diffraction pattern of $La_{0.8}Ca_{0.2}MnO_3$ and $La_{0.8}Ce_{0.2}MnO_3$.

doped $La_{0.8}Ce_{0.2}MnO_3$ manganites. We show that the overall features are very similar for both kinds of doping. A detailed analysis of the electrical resistivity, magnetic susceptibility and thermopower suggests that both divalent and tetravalent doping produce ferromagnetic metallic states, and besides the electron–phonon effect another possibility for the change in carrier density arises due to the presence of electron correlation in the metallic system.

2. Experiment

The polycrystalline $La_{1-x}Ca_xMnO_3$ and $La_{1-x}Ce_xMnO_3$ ($x = 0.2$) samples were prepared by solid-state synthesis [13]. Stoichiometric amounts for La_2O_3, $CaCO_3$, CeO_2 and MnO_2 were mixed and heated at different temperatures (950, 1050, 1250 and 1350 °C) in air for 24 h with intermediate grindings. Single-phase materials were obtained only at 1350 °C. The pellets were finally annealed at 1000 °C in oxygen atmosphere. The powder x-ray patterns were recorded using a Rigaku diffractometer with Cu Kα radiation and scanning (0.01 step in 2θ) over the angular range 10°–80°. Both the powder patterns could be indexed in the orthorhombic system. The stoichiometry of the samples prepared is confirmed by energy dispersive x-ray diffraction shown in figure 1. No impurity is detected by energy dispersive x-ray analysis (EDAX) either, and it gives expected cationic compositions. The atomic percentages are the following: La—
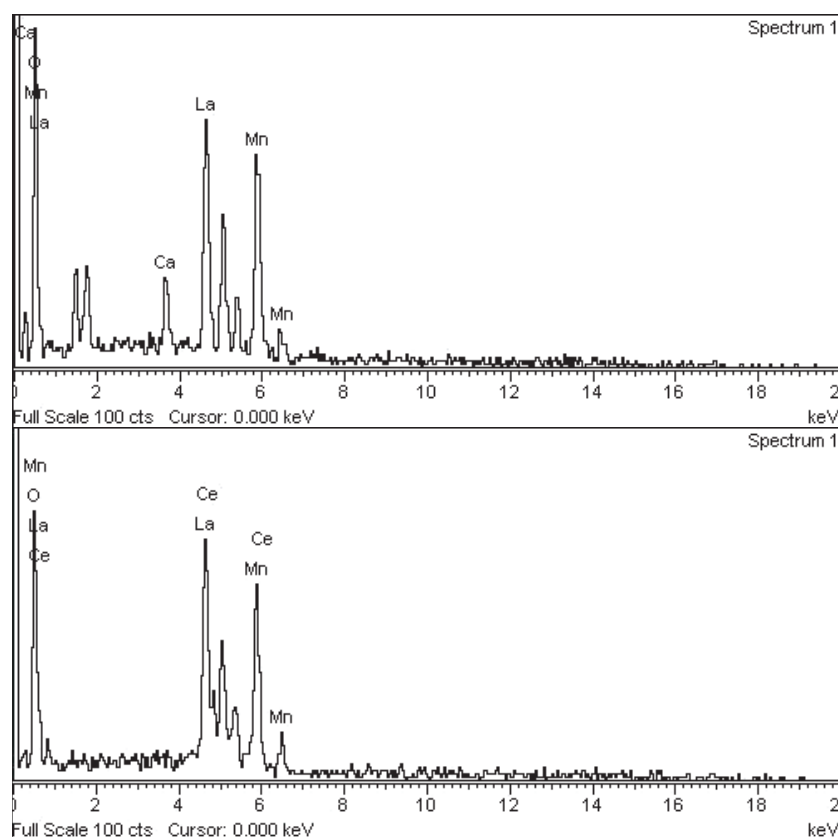
Figure 2. EDAX spectrum of $La_{0.8}Ca_{0.2}MnO_3$ and $La_{0.8}Ce_{0.2}MnO_3$ in atomic percentage.

10.55%, Ca—2.52%, Mn—14.02%, O—72.90% in $La_{0.8}Ca_{0.2}MnO_3$ and La—13.18%, Ce—4.13%, Mn—16.00%, O—66.69% in $La_{0.8}Ce_{0.2}MnO_3$, respectively figure 2.

Electrical resistivity data were obtained by a standard four-probe method. Magnetic susceptibility measurements were made using a home-made vibrating sample magnetometer set-up [14] in the temperature range of 77–300 K with accuracy better then 50 mK. We have used a Stanford Research Systems lock-in amplifier (model SR 850) and commercial Lakeshore controllers (model DCR93CA). The thermopower measurements of the doped manganite compounds have been made down to 4 K using a two-stage closed cycle refrigerator. The thermopower sample holder consists of two copper blocks electrically insulated from rest of the system but thermally connected to the cold head of the closed cycle refrigerator. The radiation shield and the vacuum of 10^{-5} mbar ensure minimal heat leak.

The temperature of one block is measured using a silicon diode sensor with a Lakeshore temperature controller. The sample is kept in between the copper blocks. A finite temperature difference of 1–2 K is maintained between the two copper blocks by a manganin wire heater wound on the copper blocks and controlled using an Au–Fe (7%)–chromel thermocouple and a Lakeshore temperature controller. The thermo-emf thus developed across the sample is measured against copper. The thermopower is computed as the ratio of the thermo-emf to the temperature difference. The absolute thermopower is then calculated by subtracting the measured thermopower from the copper thermopower.
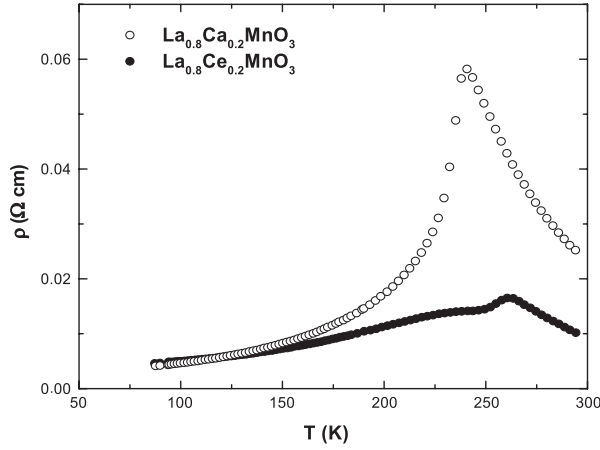
Figure 3. Temperature dependence of electrical resistivity of La$_{0.8}$Ca$_{0.2}$MnO$_3$ (open circles) and La$_{0.8}$Ce$_{0.2}$MnO$_3$ (closed circles).

3. Results and discussion

3.1. Electrical resistivity

The variation of resistivity with temperature is shown in figure 3 for La$_{0.8}$Ca$_{0.2}$MnO$_3$ and La$_{0.8}$Ce$_{0.2}$MnO$_3$. The resistivity shows a metal–insulator phase transition at $T_m = 240$ K for La$_{0.8}$Ce$_{0.2}$MnO$_3$ and $T_m = 260$ K for La$_{0.8}$Ca$_{0.2}$MnO$_3$. Further, we have noticed an extra bump above 200 K for the La$_{0.8}$Ce$_{0.2}$MnO$_3$ electron-doped system. The above feature is not intrinsic in nature and a possible reason might be due to the inhomogeneity present in the polycrystalline sample. In the present investigation, we have explored the possibility of high-energy optical phonons in order to estimate the temperature-dependent resistivity using a Bloch–Gruneisen model of resistivity.

To have a quantitative viewpoint of the measured results, the electrical transport data of La$_{0.8}$Ca$_{0.2}$MnO$_3$ and La$_{0.8}$Ce$_{0.2}$MnO$_3$ were analysed theoretically and the possibility of high-energy optical phonons explored in order to estimate the temperature-dependent resistivity using the Bloch–Gruneisen model. We start with a general expression for the temperature-dependent part of the resistivity, given by [15]

$$\rho \approx \left(\frac{3}{\hbar e^2 v_F^2} \right) \frac{k_B T}{M v_s^2} \int_0^{2k_F} |v(q)|^2 \left[\frac{(\hbar\omega/k_B T)^2 \, q^3 \, \mathrm{d}q}{(\exp(\hbar\omega/k_B T) - 1)(1 - \exp(-\hbar\omega/k_B T))} \right]. \tag{1}$$

$v(q)$ is the Fourier transform of the potential associated with one lattice site and v_s the sound velocity. Equation (1) in terms of acoustic phonon contribution yields the Bloch–Gruneisen function of temperature-dependent resistivity [15]:

$$\rho_{ac}(T, \theta_D) = 4A_{ac}(T/\theta_D)^4 \times T \int_0^{\theta_D/T} x^5 (e^x - 1)^{-1} (1 - e^{-x})^{-1} \, \mathrm{d}x \tag{2}$$

where $x = \hbar\omega/k_B T$ and A_{ac} is a constant of proportionality. We further assume that the modelled phonon spectrum consists of two parts: an acoustic Debye branch characterized by the Debye temperature θ_D and an optical peak defined by the Einstein temperature θ_E. In the case of the Einstein type of phonon spectrum (an optical mode) $\rho_{op}(T)$ can be described as follows:

$$\rho_{op}(T, \theta_E) = A_{op} \theta_E^2 T^{-1} \left[\exp(\theta_E/T) - 1 \right]^{-1} \times \left[1 - \exp(-\theta_E/T) \right]^{-1}. \tag{3}$$
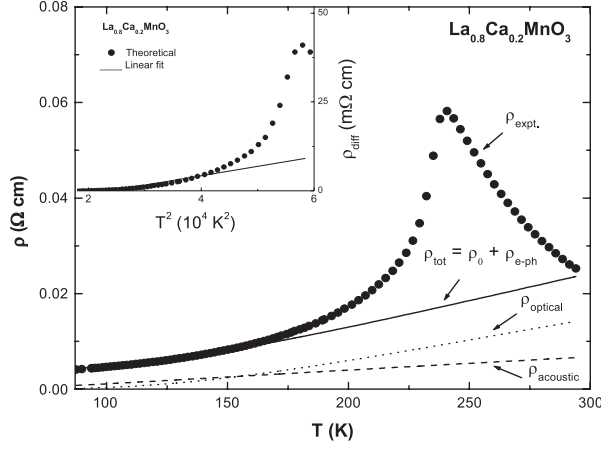
Figure 4. Variation of ρ_{e-ph} with temperature for $La_{0.8}Ca_{0.2}MnO_3$ and the contribution of acoustic phonons ρ_{ac} as well of optical phonons ρ_{op} to the resistivity. The calculated ρ_{tot} ($=\rho_0 + \rho_{e-ph}$) deviates from the measured data (closed circles) above 165 K. The inset shows the variation of ρ_{diff} ($=\rho_{exp} - \rho_{tot}$) versus T^2; a linear dependence above 165 K is clearly seen.

Figure 5. Variation of ρ_{e-ph} with temperature for $La_{0.8}Ce_{0.2}MnO_3$ and the contribution of acoustic phonons ρ_{ac} as well of optical phonons ρ_{op} to the resistivity. The calculated ρ_{tot} ($=\rho_0 + \rho_{e-ph}$) deviates from the measured data (down triangle) above 175 K. The inset shows the variation of ρ_{diff} ($=\rho_{exp} - \rho_{tot}$) versus T^2; a linear dependence above 175 K is clearly seen.
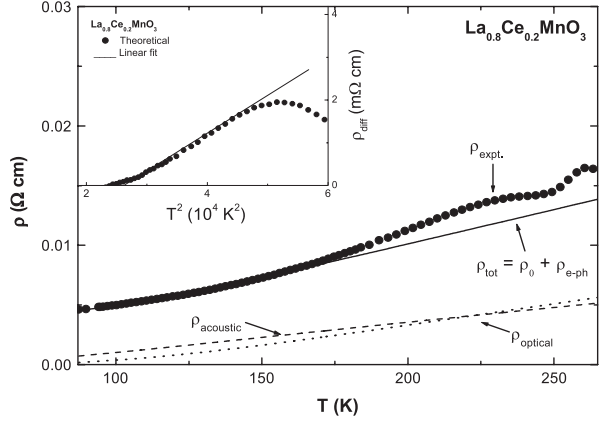
Here A_{op} is defined analogously to equation (2). Thus, the phonon resistivity can be conveniently modelled by combining both terms arising from acoustic and optical phonons,

$$\rho_{e-ph}(T) = \rho_{ac}(T, \theta_D) + \rho_{op}(T, \theta_E). \tag{4}$$

If the Matthiessen rule is obeyed, the resistivity may be represented as a sum $\rho(T) = \rho_0 + \rho_{e-ph}(T)$, where ρ_0 is the temperature-independent residual resistivity.

The resistivity curves plotted in figures 4 and 5 manifest that parts of the resistivity were determined by the electron scattering on acoustic and optical phonons, shown along with the total resistivity for $La_{0.8}Ca_{0.2}MnO_3$ and $La_{0.8}Ce_{0.2}MnO_3$. As inferred from the curve, ρ_{ac} increases rather linearly while ρ_{op} exhibits an exponential growth with temperature. Here $\theta_D = 412$ K and $\theta_E = 650$ K were taken from the reported specific heat measurements [16] and Raman spectroscopy measurements [8]. The deduced numerical results on the temperature
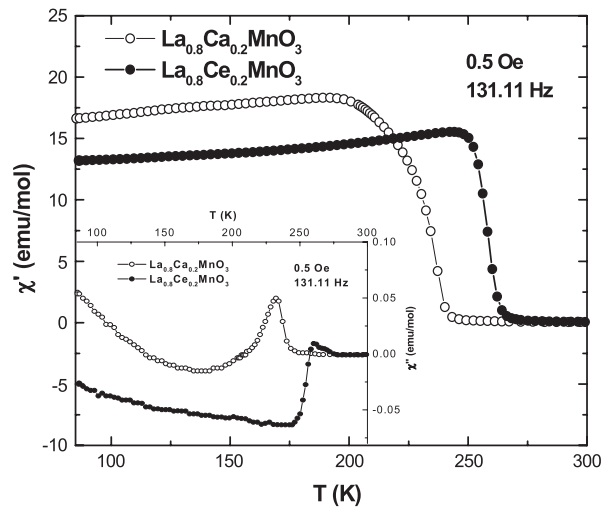
Figure 6. Low-field ac susceptibility of $La_{0.8}Ca_{0.2}MnO_3$ and $La_{0.8}Ce_{0.2}MnO_3$. The inset shows the ferromagnetic losses in the ferromagnetic phase.

dependence of resistivity of $La_{0.8}Ca_{0.2}MnO_3$ and $La_{0.8}Ce_{0.2}MnO_3$ are also given in respective figures along with the experimental data. The significant feature is that the estimated ρ is quite consistent with the experimental data at lower temperatures, but starts to deviate from the data above $T \sim 165$ K for $La_{0.8}Ca_{0.2}MnO_3$ and $T \sim 175$ K for $La_{0.8}Ce_{0.2}MnO_3$.

The difference between the measured and calculated electrical resistivity ρ_{diff} ($=\rho_{exp} - (\rho_0 + \rho_{e-ph})$) against T^2 is plotted in the inset of figures 4 and 5, where a linear variation is clearly seen above $T \sim 165$ K for $La_{0.8}Ca_{0.2}MnO_3$ and $T \sim 175$ K for $La_{0.8}Ce_{0.2}MnO_3$. Such a power law dependence of ρ_{diff} (quadratic in temperature) at higher temperatures is an indication of electron–electron scattering. The additional term due to the electron–electron contribution was required in understanding the resistivity behaviour, as extensive attempts to fit the data with residual resistivity and phonon resistivity were unsuccessful. The power temperature dependence of ρ_{diff} on electron–electron scattering was also earlier noticed in hole-doped manganites [15], cuprates [17], bismuth oxides [18], doped fullerides [19], diborides [20] and intermetallic alloys [21]. The departure from electron–phonon-induced resistivity behaviour could be ascribed to either the change in dimensionality or the change in carrier density. Our analysis of the electrical resistivity of electron and hole doped manganites suggests that besides the electron–phonon effect another possibility for the change in carrier density arose due to the presence of electron correlation in the metallic system.

3.2. Susceptibility

We have also measured the low-field (0.5 Oe) ac susceptibility to explore the magnetic phases of these samples. Figure 6 gives the temperature dependence of the real part (χ') and imaginary part (χ'') (see inset) of ac susceptibility for both samples. It is revealed that both samples undergo a transition from paramagnetic to ferromagnetic phase at a defined $T_c = 240$ K and 263 K for Ca^{2+} and Ce^{4+} doped samples, respectively. The values of T_c were determined from the inflexion points of the $\chi'(T)$ curves. We observe a systematic increase in T_c on going from doping Ca^{2+} to Ce^{4+}. Both the real part (χ') and the imaginary part (χ'') of the ac susceptibility increase sharply below T_c and show a peak just below T_c. In the inset is the imaginary part (χ'')
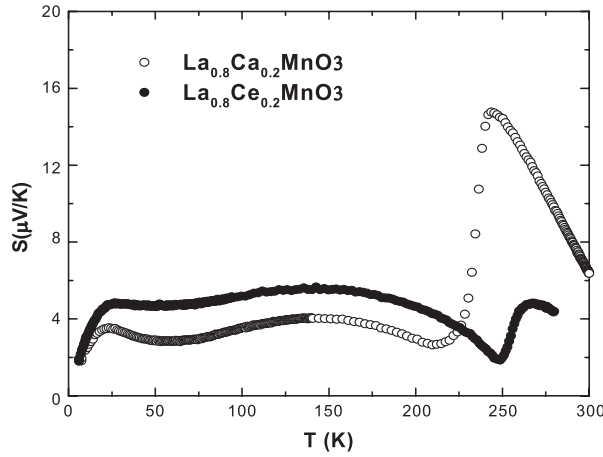
Figure 7. Thermopower as a function of temperature for the La$_{0.8}$Ca$_{0.2}$MnO$_3$ and La$_{0.8}$Ce$_{0.2}$MnO$_3$.

of the ac susceptibility showing the peaks associated with ferromagnetic losses at the respective transitions.

3.3. Thermopower

The variation of thermopower with temperature is shown in figure 7 for both samples. It is inferred that the thermopower shows a metal–insulator phase transition, manifested by a jump between metal-like behaviour at low temperature and semiconductor-like behaviour at high temperature for La$_{0.8}$Ca$_{0.2}$MnO$_3$ and La$_{0.8}$Ce$_{0.2}$MnO$_3$. Deduced values of the metal–insulator phase transition are $T_m \approx 240$ K for La$_{0.8}$Ca$_{0.2}$MnO$_3$ and $T_m \approx 263$ K for La$_{0.8}$Ce$_{0.2}$MnO$_3$, which are almost comparable with the electrical resistivity. In the paramagnetic (PM) phase, on cooling, S increases down to T_c, and then decreases very rapidly in the ferromagnetic state. Furthermore, in the low-temperature domain, S shows an upturn in the ferromagnetic phase. The small upturn at low temperatures may be due to the weak localization. A linear term and a phonon-drag-type anomaly are clearly visible at low temperatures, further evidence of well established metallic phases [15].

In the temperature range where diffusive S dominates, the S of metals, even disordered ones, is of the order of a few μV K^{-1} and is linear in temperature. The thermopower of semiconductors, in contrast, is typically several tens to hundreds of μV K^{-1}, and is governed by thermal activation of carriers, thus increasing with decreasing temperature. Henceforth, the S values of metals and non-metals differ not only in their magnitude but also in their temperature dependence. For La$_{0.8}$Ca$_{0.2}$MnO$_3$ and for La$_{0.8}$Ce$_{0.2}$MnO$_3$ in the paramagnetic insulating state we find $S \approx 6$ μV K^{-1}. It is further noticed that both these samples show a positive thermopower range up to room temperature, and this is indicative of holes as charge carriers for thermal conduction.

The measured thermopower is analysed following the Kubo formula [22]. It has contributions from both phonons and carriers. We first explore the lattice part; in the continuum approximation

$$S_{ph}^{drag}(T) = -\frac{k_B}{|e|} \left[\frac{T}{\theta_D} \right]^3 \int_0^{\omega_D} d\omega (\beta\omega)^4 A(\omega)(\beta\omega)^4 \frac{e^{\beta\omega}}{(e^{\beta\omega}-1)^2} \tag{5}$$

Table 1. Parameters of phonon drag for $La_{0.8}Ca_{0.2}MnO_3$ and $La_{0.8}Ce_{0.2}MnO_3$.

Samples	D_{phd} (10^{-8} K^{-3})	D_{phgb} (10^{-3})	D_{phph} (10^{-4} K^{-6} s^{-1})	D_{phe} (10^{-3})
$La_{0.8}Ca_{0.2}MnO_3$	5.73	3	0.1	2.3
$La_{0.8}Ce_{0.2}MnO_3$	1.4	3	0.8	9.1

with k_B the Boltzmann constant, e the charge of carriers, ω_D the Debye frequency and $\beta = \hbar/k_B T$. The relaxation time is inhibited in $A(\omega)$ and is proportional to the imaginary part of the phonon self-energy. The phonon drag thermopower relaxation time $A(\omega)$ is written as

$$A(\omega) = \frac{\left[1/\tau_{ph-d} + 1/\tau_{ph-gb} + 1/\tau_{ph-ph} + 1/\tau_{ph-c}\right]}{\left[1/\tau_{ph-d} + 1/\tau_{ph-gb} + 1/\tau_{ph-ph}\right]},$$
$$= \frac{D_{phd}(\hbar/k_B)^3\omega^4 + D_{phgb}v_s/L + D_{phph}(T\omega\hbar/k_B)^3 + D_{phc}\omega n_F}{D_{phd}(\hbar/k_B)^3\omega^4 + D_{phgb}v_s/L + D_{phph}(T\omega\hbar/k_B)^3}. \quad (6)$$

The various relaxation times are defined in terms of transport coefficients elsewhere [23]. Here, L is grain size; n_F is the Fermi–Dirac distribution function. The notations τ_{ph-d}, τ_{ph-gb}, τ_{ph-ph} and τ_{ph-c} are the phonon scattering relaxation time due to defects, grain boundaries, phonons and phonon–carrier interactions respectively. We note that to this order Matthiessen's rule holds, namely that the inverse of the total relaxation time is the sum of the various contributions for the different scattering channels. While estimating the temperature-dependent thermopower of these samples, we make use of the transport parameters, which characterize the strengths of the phonon–defect (D_{phd}), phonon–grain boundary (D_{phgb}), phonon–phonon (D_{phph}) and phonon–carrier (D_{phe}) scattering processes and are listed in table 1. These are indeed material-dependent parameters for phonon drag thermopower in the present model. We have taken the length of the sample as about 3 mm and $v_s = 3 \times 10^5$ cm s^{-1}.

The main finding of phonon drag thermopower (S_{ph}^{drag}) in figure 8 is that at low temperatures the quasi-particle excitation condensed into the ground state and they cannot scatter phonons. S_{ph}^{drag}, thus, increases exponentially with temperature in the absence of the other scattering mechanism. Although the phonon drag thermopower experiences an exponential increase at low temperature, the presence of the defects, grain boundaries and carriers set a limit on its growth; as a consequence, the phonon drag thermopower diminishes as the temperature increases further.

First it is evident from figure 8 that at low temperatures $S_{ph}^{drag}(T)$ is linear in temperature, which is common for most metals, and changes in slope around 10 K. The departure from linearity at about 10 K depends on the relative magnitudes of the phonon defect and phonon–phonon interactions. Below 10 K, the grain boundary and defects become the effective phonon scatterers and the thermopower exhibits a typical T^2 behaviour at even lower temperatures, grain-boundary scattering dominates and the usual Debye T^3 behaviour appears. $S_{ph}^{drag}(T)$ shows a saturating behaviour and shows slow negative $dS(T)/dT$ at higher temperatures. This kind of nature is attributed to the fact that the phonon mean free path decreases with the increase in temperature, as more and more carriers are available for scattering. A possible reason for the departure from linearity at about 10 K is mainly due to the competition between the increase in the phonon population and the decrease in phonon mean free path due to phonon–phonon scattering as evident from equations (5) and (6).

To ascertain the physical significance of the density of impurities, we evaluate the transport coefficients D_{phd} ($=3n_i R^2/4\theta_D^3$) appearing in equation (6). Here, n_i is the density of impurities or defects and R is the relative ionic-mass difference. We estimate the product of the
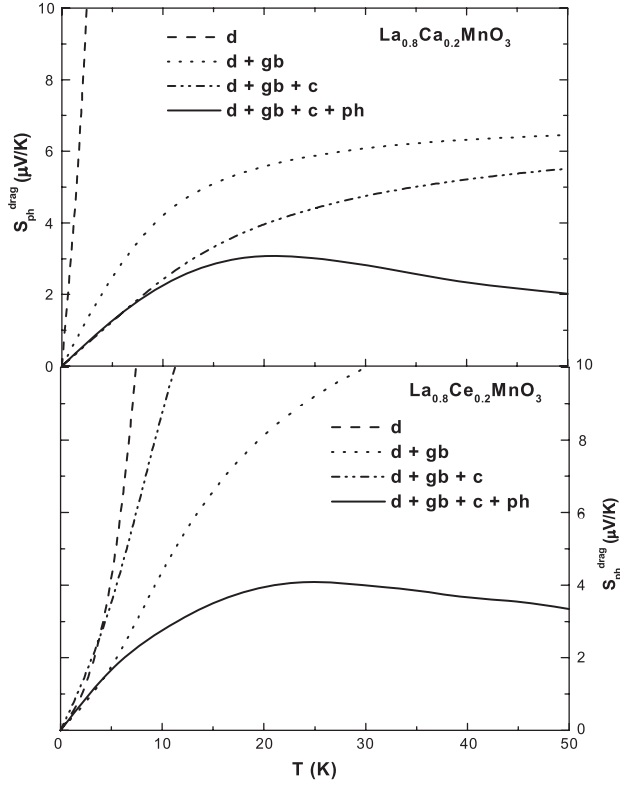
Figure 8. Variation of phonon thermoelectric power as a function of temperature in the presence of various phonon scattering mechanisms for the $La_{0.8}Ca_{0.2}MnO_3$ (upper panel) and $La_{0.8}Ce_{0.2}MnO_3$ (lower panel).

density of impurities and the square of the relative ionic mass difference, $n_i R^2$, as 5 and 1.3 for $La_{0.80}Ca_{0.20}MnO_3$ and $La_{0.80}Ce_{0.20}MnO_3$, respectively, from the value of the coefficient D_{phd}. Since transport parameter D_{phd} is determined by the magnitude of the phonon–impurity interaction, we are able to roughly estimate the density of impurity scatterers, which may point to the fact that the quasi-particles in the metallic state are essentially localized. In this way, one can set a limit to the concentration of impurities if the impurities as scatterers are isotopic in origin.

We shall now proceed to include the effect of the free carrier diffusion contribution towards the thermoelectric power employing the well known Mott formula. The low-temperature carrier diffusion thermoelectric power [24] is

$$S_c^{diff}(T) = -\frac{\pi^2 k_B^2 T}{3|e|}\left[\frac{\partial \ln \sigma(\varepsilon)}{\partial \varepsilon}\right]_{\varepsilon=\varepsilon_F} \tag{7}$$

with $\sigma(\varepsilon)$ $(=Ne^2\tau(\varepsilon_F)/m)$ the energy dependence of the conductivity in the relaxation time approximation. For the sake of simplicity, the mean free path of the carriers (ℓ) is assumed to be independent of temperature; equation (7) becomes

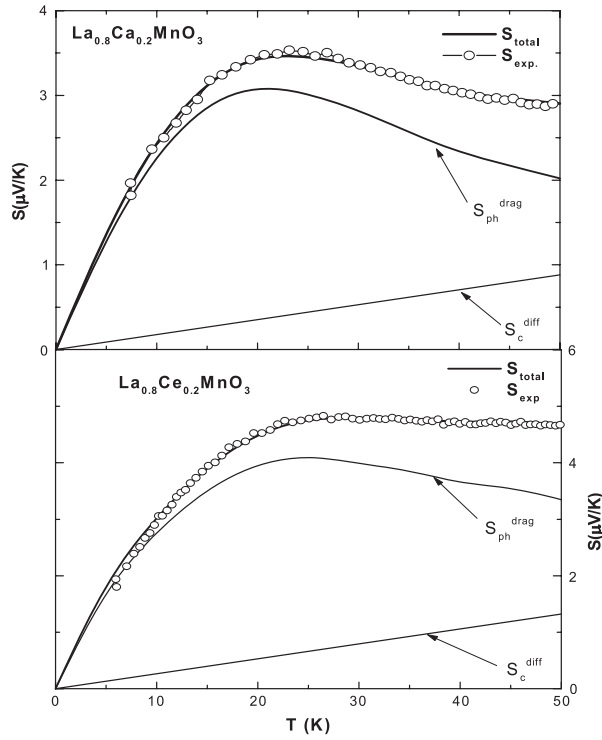$$S_c^{diff}(T) = -\frac{\pi^2 k_B^2 T}{3|e|\,\varepsilon_F}. \tag{8}$$

Figure 9. Thermopower versus temperature along with experimental data. Upper panel and lower panel for $La_{0.8}Ca_{0.2}MnO_3$ and $La_{0.8}Ce_{0.2}MnO_3$, respectively.

For constant mean free path, the method points to the scattering of carriers by impurities as dominant. The effective mass of the carriers along the Mn–O plane is obtained from the electronic specific heat coefficient, γ, using the relation $m^* = 3\hbar^2\gamma d/\pi k_B^2$. Considering $\gamma = 4.7$ mJ mol^{-1} K^{-2} from the heat capacity measurement [16], $m^* \cong 2.4 m_e$ is obtained. For a stack of 2D conducting planes well separated by an average spacing, d, the condition for optimized transfer of electrons implies the 2D electronic charge carrier density and follows $n_c d^2 = 1$ to obtain $n_c \cong 2.2 \times 10^{14}$ cm^{-2}. Analogously, we express the 3D electronic charge carrier density following $n_v d^3 = 1$ to obtain $n_v \cong 5.65 \times 10^{21}$ cm^{-3}. Within the Fermi liquid picture the calculated electron parameter is the Fermi energy $\varepsilon_F \cong 0.6$ (0.4) eV for $La_{0.80}Ca_{0.20}MnO_3$ and $La_{0.80}Ce_{0.20}MnO_3$, respectively.

To gain an additional insight into the observed metallic behaviour, it is worth addressing the possible role of mass renormalization of carriers due to differing values of γ obtained from electron energy band structure calculation [25] and specific heat measurements [16]. In this situation it is worth addressing the role of Coulomb correlations in revealing the transport properties in manganites. In fact, the effective charge carrier mass is sensitive to the nature of interaction in the Fermi liquid description.

In the present analysis of the elastic carrier–impurity contribution to the thermopower figure 9 is plotted for $La_{0.80}Ca_{0.20}MnO_3$ and $La_{0.80}Ce_{0.20}MnO_3$ along with the experimental data. The thermopower behaviour depends on the competition among the various scattering mechanisms for the heat carriers and the balance between the electron and phonon competition. Finally, it is worth stressing that the $S(T)$ decreases slowly above 25 K and is well reproduced from the present theoretical model (see figure 9); this phenomenon is attributed to shortened

phonon mean free path as compared to that at low temperatures. It may be seen that the slope change in S_{ph}^{drag} is much more pronounced than that in S_c^{diff} below 15 K for both samples. The reason for this change is the fact that the phonon–impurity scattering dominates and the electron–impurity scattering is weaker.

4. Conclusions

In conclusion, we have measured transport properties of hole (Ca) and electron (Ce) doping of LaMnO$_3$ manganites. The x-ray diffraction pattern and EDAX confirm the single phase and stoichiometry of polycrystalline samples of La$_{0.8}$Ca$_{0.2}$MnO$_3$ and La$_{0.8}$Ce$_{0.2}$MnO$_3$. The electrical resistivity and thermopower data show a metal–insulator phase transition for both samples. Magnetic susceptibility measurement confirms that both the samples undergo a transition from paramagnetic to ferromagnetic phase at a well defined Curie temperature (T_c). In the case of the hole-doped manganites the double exchange mechanism involving Mn^{3+} and Mn^{4+} is invoked to explain the CMR. The mechanism is caused by the Jahn–Teller ion Mn^{3+} and is not related to non Jahn–Teller ions Mn^{4+} and Mn^{2+}. Analogous to the hole-doped La$_{1-x}$Ca$_x$MnO$_3$ one could also have double exchange between Mn^{3+} and Mn^{2+} in electron-doped La$_{1-x}$Ce$_x$MnO$_3$ giving rise to ferromagnetism, where we partially replace Mn^{3+} (Jahn–Teller ions) by Mn^{2+} ions.

Theoretically analysed electrical resistivity within the framework of the classical electron–phonon model of resistivity, i.e. the Bloch–Gruneisen model, shows that the estimated ρ is quite consistent with the experimental data at lower temperatures with electron–phonon scattering, but starts to deviate at higher temperatures. The difference between the measured and calculated electrical resistivity shows quadratic temperature dependence at higher temperatures and is an indication of electron–electron scattering. The departure from electron–phonon-induced resistivity behaviour could be ascribed to either the change in dimensionality or the change in carrier density. Our analysis of the electrical resistivity of electron- and hole-doped manganites suggests that besides the electron–phonon effect another possibility for the change in carrier density arises due to the presence of electron correlation in the metallic system.

In order to simulate the actual situation occurring in the temperature-dependent behaviour of $S(T)$ in manganites, we considered two channels to $S(T)$: carrier diffusion (S_c^{diff}) and phonon drag (S_{ph}^{drag}) within the relaxation time approximation. The phonon drag (S_{ph}^{drag}) is discussed within the Debye-type relaxation rate approximation in terms of the acoustic phonon frequency, a relaxation time τ and the sound velocity. The rapid increase in $S(T)$ is attributed to increase in phonon mean free path due to carrier condensation in the low-temperature domain limited by various impurity scattering mechanisms. The physical entities in the present scheme that characterize the strengths of the phonon–defect, phonon–electron and phonon–phonon scattering lead to a result that successfully reproduces the experimental curve. The behaviour of the $S(T)$ is determined by competition among the several operating scattering mechanisms for the heat carriers and a balance between carrier diffusion and phonon drag contributions in the polycrystalline samples of hole-doped La$_{0.8}$Ca$_{0.2}$MnO$_3$ and electron-doped La$_{0.8}$Ce$_{0.2}$MnO$_3$ manganites.

12

References

[1] Salamon M B and Jaime M 2001 *Rev. Mod. Phys.* **73** 583
[2] Zener C 1951 *Phys. Rev.* **82** 403
[3] Millis A J, Littlewood P B and Shrainman B I 1995 *Phys. Rev. Lett.* **74** 5144
[4] Jaime M, Lin P, Salamon M B and Han P D 1998 *Phys. Rev.* B **58** R5901
[5] Urushibara A, Moritomo Y, Arima T, Asamitsu A, Kido G and Tokura Y 1995 *Phys. Rev.* B **51** 14103
[6] Kubo K and Ohata N 1972 *J. Phys. Soc. Japan* **33** 21
[7] Zhao G-M, Smolyaninova V, Prellier W and Keller H 2000 *Phys. Rev. Lett.* **84** 6086
[8] Abrashev M V, Avanov V G, Iliev M N, Chakalov R A, Chakalova R I and Thomsen C 1999 *Phys. Status Solidi* b **215** 631
    Abrashev M V, Litvinchuk A P, Iliev M N, Meng R L, Popov V N, Ivanov V G, Chakalov R A and Thomsen C 1999 *Phys. Rev.* B **59** 4146
[9] Maignan, Martin C, Damay F, Raveau B and Hejtmanek 1998 *Phys. Rev.* B **58** 2758
[10] Mandal P and Ghosh B 2003 *Phys. Rev.* B **68** 014422
[11] Fisher B, Patlagan L, Reisner G M and Knizhnik A 1997 *Phys. Rev.* B **55** 9227
[12] Hundley M F and Neumeier J J 1997 *Phys. Rev.* B **55** 11511
[13] Topfer J and Goodenough J B 1997 *Solid State Chem.* **130** 117
[14] Bajpai A and Banerjee A 1997 *Rev. Sci. Instrum.* **68** 11
[15] Varshney D and Kaurav N 2004 *Eur. Phys. J.* B **37** 301
[16] Ghivelder L, Castillo I A, Alford N M, Tomka G J, Riedi P C, MacManus-Driscoll J, Akther Hossain A K M and Cohen L F 1998 *J. Magn. Magn. Mater.* **189** 274
[17] Varshney D, Choudhary K K and Singh R K 2002 *Supercond. Sci. Technol.* **15** 1119
[18] Varshney D, Shah S and Singh R K 1998 *Superlatt. Microstruct.* **24** 4099
[19] Varshney D, Kaurav N and Choudhary K K 2005 *Supercond. Sci. Technol.* **18** 1259
[20] Varshney D 2006 *Supercond. Sci. Technol.* **19** 685
[21] Kuo Y K, Sivakumar K M, Tasi J I, Lue C S, Huang J W, Wang S Y, Varshney D, Kaurav N and Singh R K 2007 *J. Phys.: Condens. Matter* **19** 176206
[22] Callaway J 1991 *Quantum Theory of the Solid State* (London: Academic)
[23] Varshney D 2006 *Supercond. Sci. Technol.* **19** 433
    Varshney D and Kaurav N 2007 *J. Low Temp. Phys.* **147** 7
[24] Mott N F and Davis E A 1979 *Electronic Processes in Non-Crystalline Materials* (Oxford: Clarendon)
[25] Pickett W E and Singh D J 1996 *Phys. Rev.* B **53** 1146